# QUANTITATIVE PREDICTION OF

# DYE FLUORESCENCE QUANTUM YIELDS IN PROTEINS

by

Ryan Mitchell Hutcheson

A thesis submitted in partial fulfillment
of the requirements for the degree

of

Master of Science

in

Chemistry

MONTANA STATE UNIVERSITY
Bozeman, Montana

May 2009

APPROVAL

of a thesis submitted by

Ryan Mitchell Hutcheson

This thesis has been read by each member of the thesis committee and has been found to be satisfactory regarding content, English usage, format, citation, bibliographic style, and consistency, and is ready for submission to the Division of Graduate Education.

Patrik R. Callis, PhD

Approved for the Department of Chemistry and Biochemistry

David Singel, PhD

Approved for the Division of Graduate Education

Dr. Carl A. Fox

# STATEMENT OF PERMISSION TO USE

In presenting this thesis in partial fulfillment of the requirements for a master's degree at Montana State University, I agree that the Library shall make it available to borrowers under rules of the Library.

If I have indicated my intention to copyright this thesis by including a copyright notice page, copying is allowable only for scholarly purposes, consistent with "fair use" as prescribed in the U.S. Copyright Law. Requests for permission for extended quotation from or reproduction of this thesis in whole or in parts may be granted only by the copyright holder.

Ryan Mitchell Hutcheson

May 2009

# DEDICATION

To my friends and family, without whom I could not have accomplished the tasks set before me. I would especially like to thank my wife and son, for they have made my life such a joy. I would also like to thank Ramon Tusell for the many discussions about rate constant calculations and for being a good friend.

TABLE OF CONTENTS

# LIST OF TABLES

# LIST OF FIGURES

LIST OF FIGURES – CONTINUED

Figure Page

# ABSTRACT

The application of a method previously developed by Callis et al. to predict the quantum yields of Trp fluorescence has been successfully applied to the fluorescence of fluorescein and flavins in proteins. The calculated lifetime range of 2 ps – 4 ns is in agreement with experiment.

The fluctuations in the electron transfer rate are shown to be dictated by the fluctuations in the density of states. This is evident by the comparison of the fractional deviation of the interaction, density of states and the rate. Here the fluctuations in the density of states is an order of magnitude larger than the fluctuations in the interactions and is nearly the same as that of the $k_{ET}$ fluctuations. This demonstrates that the fluorescence lifetime variability is controlled by the electrostatic environment and not the distance dependence of the interaction.

# INTRODUCTION

## History of Tryptophan Fluorescence

Tryptophan (Trp) fluorescence has been extensively used to track the changes in protein, both physical and chemical. Trp has been used primarily because of the great sensitivity of the fluorescence lifetime ($\tau_f$), intensity/quantum yield ($\varphi_f$), and wavelength to the protein environment. The fluorescence quantum yields vary from about 0.35 down to ~0.01, depending on the protein environment[1]. This is amazing because the light absorbing part, 3-methlyindole (3MI), shows very little variability in $\varphi_f$ when dissolved in different solvents varying in polarity, always being around 0.3[2].

It was well accepted early on that electron transfer (ET) from the indole ring to the amide was the cause of the variation because N-acetyltryptophanamide (NATA), whose only apparent quenching mechanism is an ET to an amide group ($\varphi_f$=0.14 vs. 0.34 for 3MI in water) is similar to that of Trp in protein environments, where the indole ring is always near an amide. However, the poor electron accepting abilities of amides raises the question of how the amide is able to quench Trp.

While most of the explanation has focused on the electronic coupling parameter ($V^2$) and its exponential dependence on distance[3-5], little attention had been given to the parameters associated with the activation energy. This left a substantial hole in a comprehensive explanation of these variations until recently when Callis et al.[6-9] was able to explain the phenomenon from the activation energy.

Callis and coworkers[6-9] recently made significant progress in explaining the wide variation in both the quantum yield and the nonexponential decay of Trp in proteins. This was done by considering only the activation energy. The assumption was made that the electronic coupling constant would be nearly constant because the indole ring is never more than 4-6Å away from the nearest amide and therefore not the limiting step. They also emphasized that Marcus theory states that ET can only occur if the fluorescing state and Franck Condon accessible vibrational level of the charge transfer state are in resonance with each other[10].

Callis, Vivian, and Liu[6-9] calculated the energy transitions for the charge transfer (CT), the fluorescing ($S_1$) states, the reorganization (CT relaxation) energy, as well as the Franck-Condon factors (FC). This was done for several proteins; two are shown in Figure 1. From this, they could calculate the quantum yield using Fermi's Golden Rule as described in the methods.

Values of $k_{rad} = 4 \times 10^7\ s^{-1}$ and $k_{nr} = 8 \times 10^7\ s^{-1}$ for Trp in water were taken from Yu et al[11]. These values give a quantum yield of 0.33 for Trp in water in the absence of a quencher. Experimental ET rates were calculated using the known quantum yield of each protein and equation 5.

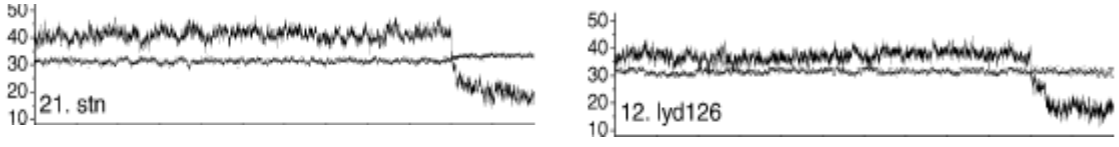


Figure 1[7]: Two example trajectories run by Callis and Liu. A is an example of a high quantum yield protein. B is an example of a low quantum yield protein. The top line in each is the CT energy transition, the bottom line is the $S_1$ energy and the drop in CT energy in the reorganization energy (λ). Both are a plot of transition energy ($kcm^{-1}$) vs. time (ps).

Using calculated parameters for the transition energies for the CT and $S_1$ state, as well as the reorganization energy, and the Franck-Condon factors, a global fit for V of 10cm$^{-1}$ for every case, and an offset for the $\Delta E_{00}$ of -4000cm$^{-1}$, Callis et al.[7] were able to empirically determine the quantum yield for the various proteins.

The calculated quantum yield, as seen in Figure 2a, matches well with the experimental quantum yield, with few exceptions. The quantum yield also matches with the CT transition energy; as the CT energy decreases, so does the calculated quantum yield. Another trend found was that as the average CT energy dropped, so did the calculated quantum yield.

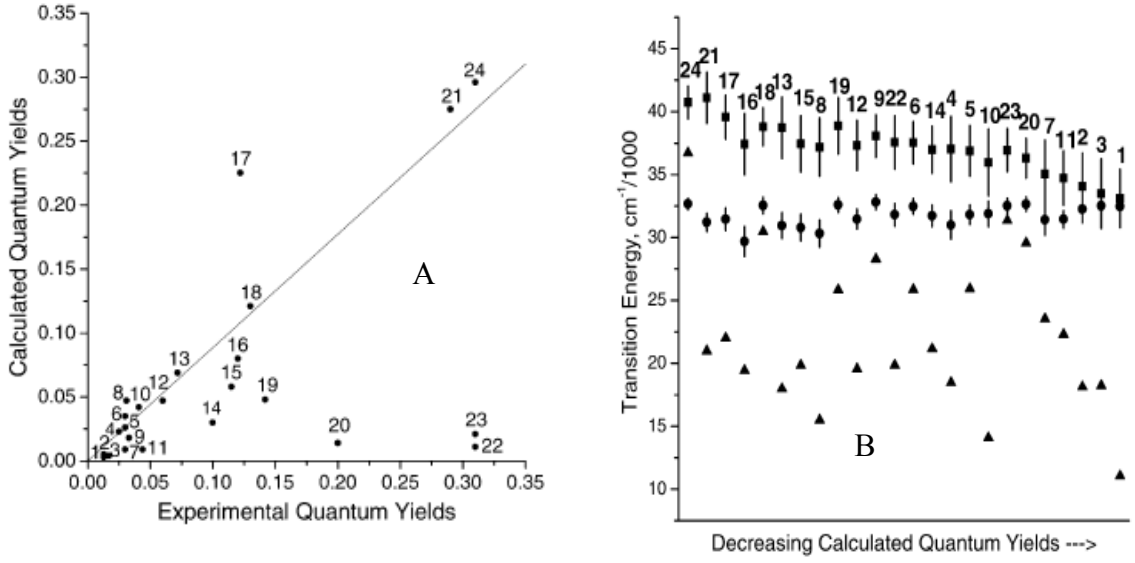


Figure 2[7]: a) Experimental vs. Calculated quantum yields of Trp. Line represents an exact match. b) Transition energy vs. decreasing quantum yield. Squares represent the CT energy, circles represent the $S_1$ energy and the triangles represent the CT relaxation, λ.

Upon examination of the crystal structures of the proteins in question, Callis and coworkers also generally saw that the proteins with a low (high) quantum yield had a negative (positive) charge closer to (farther from) the indole ring and/or a positive

(negative) charge farther from (closer to) the amide group. This would serve to create a more (less) favorable environment for ET by forcing an electron toward (away) from the amide group. In conclusion they said that the variation in quantum yield could be quantitatively explained by the change in the electric potential around the Trp.

In later studies the importance of the electric field around the Trp was confirmed when Callis et al[8] was able to explain why the placement of a fluorine atom on the indole ring reduced the fluorescence sensitivity to various protein environments, first observed Broos et al[12]. Callis rationalized that the electron affinity of the fluorine was able to pull the electron density away from the ring, creating a positive charge on the ring. This prevented an electron from leaving the ring. As a result, the sensitivity of Trp to the various protein environments nearly vanished and the lifetime remained nearly constant.

## History of Dye and Cofactor Fluorescence

The fluorescence of "dyes" and protein cofactors (such as oxidized flavins) has not been studied as extensively as that of Trp or of tyrosine (Tyr) but the volume of data has grown in recent years. Cofactors have been known to participate in ET in proteins for many years but the connection to fluorescence lifetimes has remained unsolved and fluorescent tagging of proteins with various organic dyes (fluorescein and its derivatives for example) has become popular. These molecules are subject to the same variations in fluorescence, quantum yield and lifetime variability as Trp (It is important to note that in the case of flavin fluorescence, the Trp/Tyr is acting as the quencher as can be seen by Figure 3).

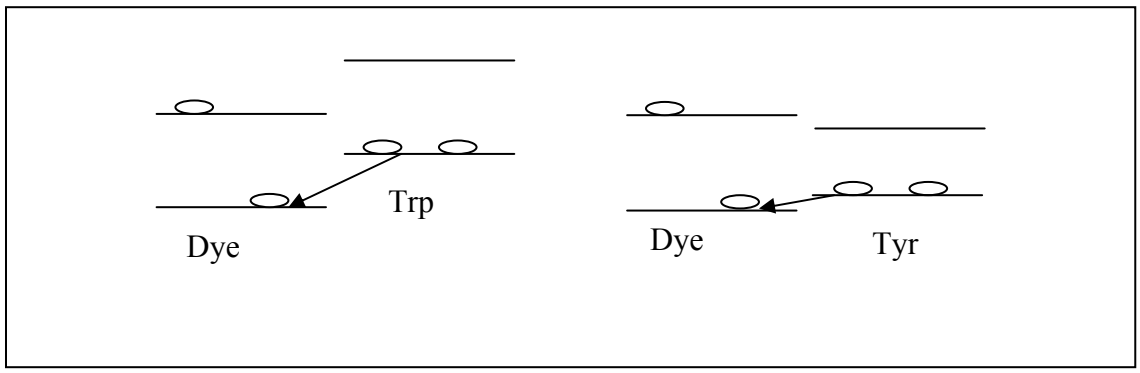


Figure 3: Cartoon of the HOMO and LUMO of two systems. a) Dye and Trp, b) Dye and Tyr.

Mataga and coworkers have recently measured the fluorescence lifetimes of oxidized flavins within proteins. In each case the oxidized flavin in the form of riboflavin (Rbf), flavin-mononucleotide (FMN), or flavin adenine dinucleotide (FAD), emits fluorescence with a lifetime on the order of 100fs to 10ps. In these cases the isoalloxazine (ISO) ring of the flavin is stacked with either one or two Trp/Tyr at the van der Waals distance[13-16]. At the shorter lifetimes (100 fs), the ET process is nearly activationless, and the rate is around $10^{13}$ $s^{-1}$.

Visser and coworkers measured the fluorescence of FAD in glutathione reductase (GR) and found that it decays almost completely in 7ps. This is despite that the nearest quencher (Tyr177) is nearly perpendicular to the ISO ring of the flavin, and the contact is only through the OH group of the Tyr[17-18].

Xie and coworkers recently did single molecule fluorescence experiments on enzymes, in which they found that the kinetics for various enzymes was not constant in time[19]. They have also done single molecule fluorescence experiments on *Escherichia coli* flavin reductase (Fre)[20] and rabbit anti-fluorescein (1FLR)[21]. In the case of the Fre, they not only found that the quenching rate was not constant in time but also that the ET

rate was relatively slow ($10^{10}$) even though the Tyr (Tyr35) within "quenching distance" of the ISO ring on FAD is within vander Waals distance, however it is not in an "ideal" sandwich orientation (Figure 10).

In the case of 1FLR, there is no clear single quencher of the fluorescein (4 Tyrs and 2 Trps within 5Å). No mutations have been done, yet Xie and coworkers say all the quenching is due to the closest Tyr (Tyr37)[21]. They concluded this because of his previous work with Fre and work done by Mataga.

This conclusion is problematic, not only because five potential possible quenchers were ignored, but also because Trp is known to be a better quencher than Tyr, due to a high lying HOMO (see Figure 5). Also, a previous study of anti-fluorescein[22-23] concluded that tryptophan was the most probable quencher, where they showed that Trp is a better quencher of aqueous fluorescein than Tyr.

Another problem with 1FLR is that fluorescein will undergo self quenching depending on the protonation state. The fluorescence quantum yield of fluorescein is highly pH dependent. Fluorescein has four protonation states: cationic (pKa=2.08, $\varphi_{fl}$=0), neutral (pKa=4.31, $\varphi_{fl}$=0), anionic (pKa=6.43, $\varphi_{fl}$=0.37), and dianionic ($\varphi_{fl}$=0.93); each with a different quantum yield. There is evidence that while the cation and neutral species do not fluoresce, they do undergo fast deprotonation to give the anion, which does fluoresce[24]. This further complicates the fluorescence spectra.

Nagano and coworkers recently modified the benzene moiety on fluorescein to determine how this would affect the quantum yield and fluorescence lifetime. They found that as the oxidation potential of the benzene moiety becomes more positive, the

yield decreases[25]. They later found that as the reduction potential became more negative, the yield increases[26]. These results suggest that the benzene moiety can either accept an electron or donate an electron, depending on the electric field around the moiety.

In both cases Xie describes the quenching as only due to $V^2$ and its exponential dependence on distance[20,21,27]. This assumes that the ET rate is activationless or that the activation energy is relatively constant with time.

This can be seen from eqn. 3 in the methods; if the assumption is made that the activation energy is constant and the exponential term can be considered a constant.

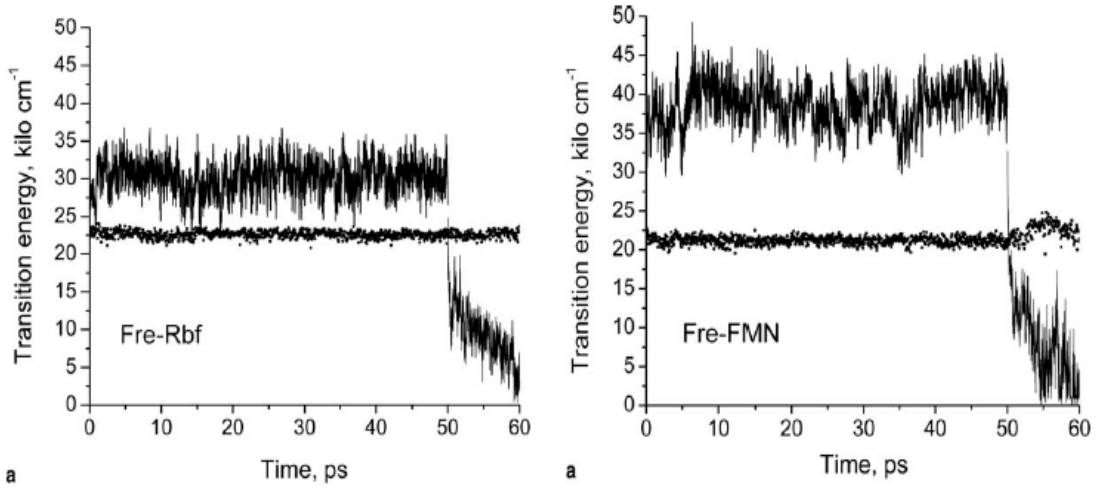


Figure 4[6]: Plot of CT and $S_1$ transition energies vs. time for Fre-Rbf and Fre-FMN.

This only leaves $V^2$ as a parameter for ET rate determination.

Liu and Callis, with Mataga's work in mind, looked at the energy gap and relaxation energy of these systems[6].

As can be seen by Figure 4, of the two cases with Fre (Rbf, FMN), only the one case can be assumed to be activationless, but neither have to be.

## Objectives

This Thesis will show that the QM-MM machinery used for the tryptophan (Trp) fluorescence studies can be used for the systems of dyes and cofactors in proteins; in this application Trp and tyrosine (Tyr) will be treated as quenchers instead of quenchees. Using the trajectories, the calculation of the configuration interaction (CI) Hamiltonian between the fluorescing state and the CT state of the dye/residue pair and the Franck-Condon factors for the intramolecular geometry changes associated with the electron transfer a rate constant can be calculated. This has been done for the three potential flavins in flavin reductase (Fre) and for six Trp/Tyr residue-fluorescein pairs in the fluorescein antibody (1FLR). The separation of the interaction and activation components of electron transfer and the determination of which component is dominant the electron transfer process has been done as well.

# METHODS

## Quantum Mechanics and Molecular Dynamics (QM-MM/MD)

An analogous form of the QM-MM method previously used by Callis et al.[6-8] was used for transition energy predictions for ET quenching by Trp/Tyr of the dyes. The QM part is Zerner's INDO/S-CIS (Zindo) method[27], modified to include the local electric field and potentials[29-30]. The MM part is Charmm (version 31b)[31]. The QM part includes the Trp/Tyr ring, the beta-carbon, the Trp/Tyr amide and that of the preceding residue, and includes the ISO ring of the flavin or the xanthene (Xan) ring of fluorescein (Flu). The Trp/Tyr is capped with hydrogens, the ISO is capped with a methyl, and the xanthene is capped with a hydrogen, so that the QM part is N-formyltryptophanamide

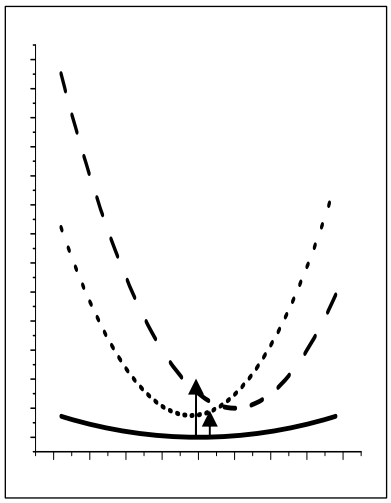

Figure 5: Potential well diagram of the ground (solid), $S_1$ (dots), CT (dash). The vertical transitions are calculated using ground state geometries.

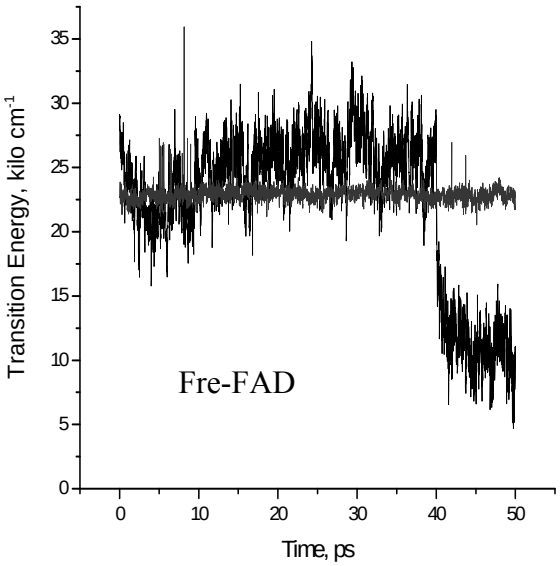


Figure 6[9]: Plot of the $S_1$ and CT transition energies vs. time.

(N-formyltyrosineamide) and ISO/xanthene[6]. The program will detect CT states when the Trp/Tyr ring is either the electron donor or acceptor.

It is important to note the transition energies of the dye and residue "sandwiches" are calculated using the ground state geometries. This artificially raises the calculated transition energies of both the $S_1$and CT states, but by different factors (Figure 5). Another important factor in the trajectories is that the charges placed on all the atoms are the $S_1$ state charges. At an arbitrary time (one of our choosing), the charges are switched to that of the CT state. This results in a relaxation of the CT state, compared to the $S_1$ state (see Figure 6).

## Optimization of Geometries for Use in the QM-MM/MD Simulations

In order to run the simulations new geometries for the dyes had to be created and optimized, this was done using Gaussian03[32]. Hartree-Fock (HF) and singles configuration interactions (CIS) calculations were used for the ground and excited states (S1 and CT) respectively. These calculations were done with the 3-21G basis set, which has been shown to give good geometry differences for indole[33-35] and now dyes by replicating the fluorescence spectra (Figure 7).

Each atom in the dyes was assigned an "atom type", specifying the environment of that atom. For example, a carbon in an aromatic ring would have a label of CA whereas a carboxylic carbon would have the designation CD. The corresponding bond lengths, strengths, angles, and dihedrals for each atom and/or group of atom types were inputted into a parameter file for use in the simulations.

A topology file had to be generated as well to include the atom charges, connectivity and atomic masses. Charges from atoms in already supplied Charmm molecules and residues were used as a starting point for atom charges in new molecules. The charges were then scaled to fit (1) the overall charge of the molecule and (2) the local environment of the specific atom. \

## Franck-Condon Factors

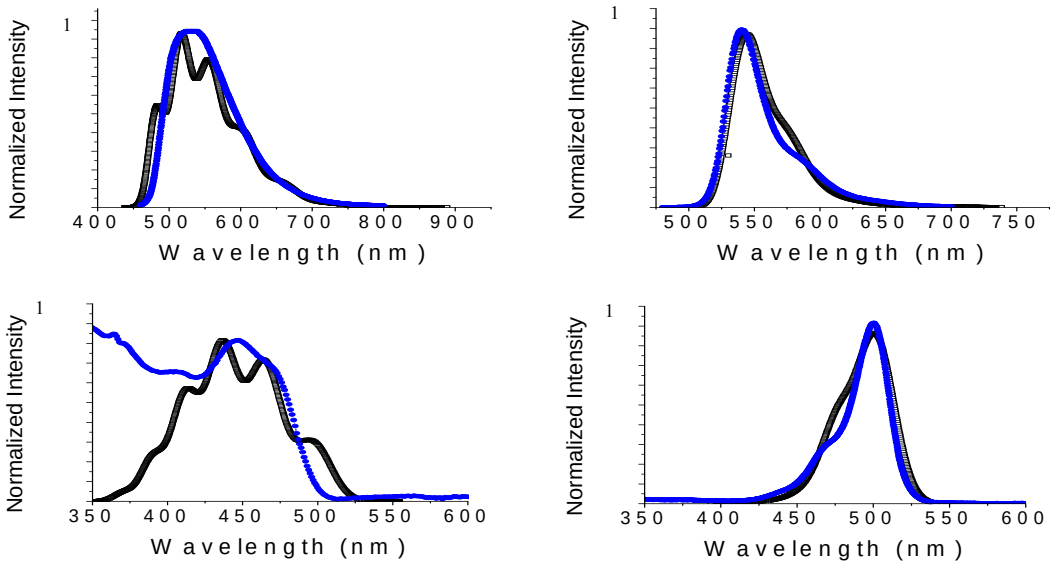


Figure 7: Duplication of the room temperature fluorescence (top) and absorption (bottom) of flavins (left) and fluorescein (right). Black lines are calculated and the blue lines are measured spectra taken from Photochem CAD.

In the case of calculating Franck-Condon factors and vibrational reorganization energies, the difference in ground and excited state geometries is of importance. A basis

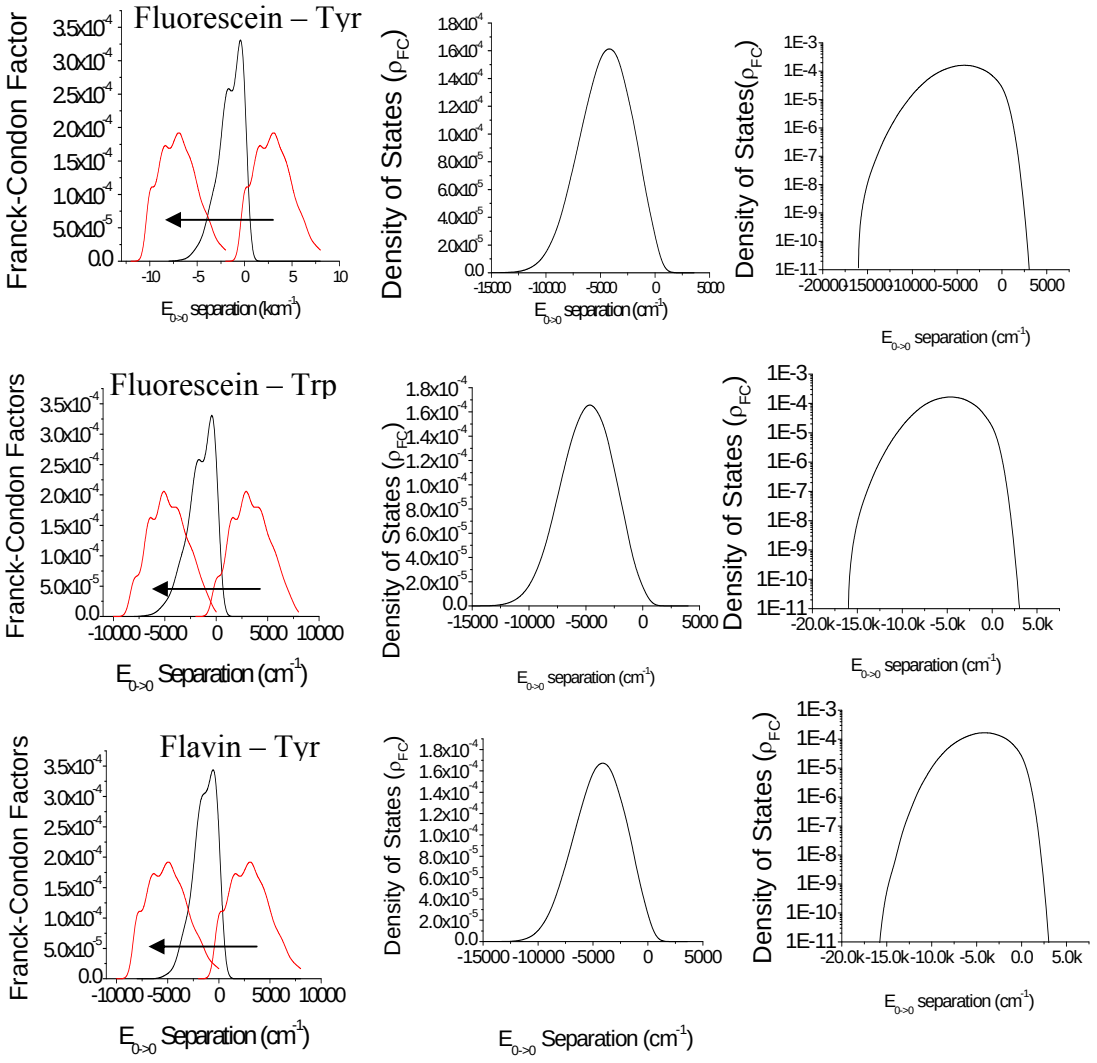


Figure 8: Franck-Condon factors (left) for the electron attachment of dye (black) and the ionization of Tyr/Trp (red). As one curve is moved relative to the other, the area under the overlap integral of the curves produces the Franck-Condon factors for the $S_1$-CT transition (middle). Semi-log plot of the density of states (right).

set of 3-21G has been shown to provide good geometry differences[33-34,36] for indole and the same is true for the dyes, as is evident by the replication of the absorption and fluorescence spectra in Figure 7. The $S_1$-CT overlap integral was calculated by

following a method used in previous studies[33-34,36] with one difference, a direct product space of the normal modes was taken for the two components independently (Trp/Tyr and flavin, dyes, etc). The CT geometry of the dye and residue was that of the respective radicals. The vibrational frequencies and modes were computed for the ground state molecules, and determined at the UHF/6-311+g** level. These calculations are able to reproduce the low temperature fluorescence spectra of 3-methyl indole almost exactly. However, due to the lack of low temperature spectra of both fluorescein and flavins, near duplication of the room temperature spectra serves as a good indicator for the validity of this method (Figure 7). The overlap of the $(Xan^{-})^{*} + e^{-} \rightarrow Xan^{2-}$ and the $Tyr(Trp) \rightarrow Tyr^{+}(Trp^{+}) + e^{-}$ spectra give the Franck-Condon factors for the $S_1$-CT transition energies calculated by the trajectories. This is accomplished by overlaying the ground-CT Franck-Condon factors of the residue over the $S_1$-CT Franck-Condon factors of the dye (Figure 8). This overlap integral will serve as the density of states for the calculation of the rate constant[37].

## CI Hamiltonian Matrix Element

The last portion on the electron transfer rate to be calculated was the configuration interaction Hamiltonian matrix element, this was done using Gaussian03[32]. A method previously developed by Callis et al[37] to calculate the electronic coupling elements was used. Here a CIS/3-21g basis set was used to calculate the singly excited configuration interaction (CIS) Hamiltonian matrix, its eigenvalues, and its eigenvectors. This was done for a set of configurations that included several

MO's below the HOMO to several above the LUMO of the charge transfer pair every 10 fs of the trajectories. The coupling element is the singlet adapted CT Hamiltonian matrix element calculated between the configurations corresponding to the fluorescing and CT states using the following route card # hf/3-21g cis(singlet,icdiag,rw) pop=full iop(3/33=1, 6/7=0, 6/8=2,6/9=2) and using a modified L914 link, modified to output the small part of the CIS matrix needed[37].

## Electron Transfer Rate

Fermi's Golden Rule was used to calculate the electron transfer rate, wherein the transition rate for a defined initial state to a continuum of final states of the same energy is given by[38]:

$$T_{f\to i} = \left(\frac{2\pi}{\hbar}\right)\left|\langle f|H|i\rangle\right|^2 \rho, \qquad (1)$$

where $\langle f|H|i\rangle$ is the matrix element of the perturbation, $H$, between the final and initial states and ρ is the density of final states. A useful form of this rule is given by:

$$k_{ET} = 4\pi^2 c V^2 \langle \rho_{FC} \rangle \qquad (2)$$

(all energies are expressed as wave numbers, $cm^{-1}$) where $c$ is the speed of light, $V$ is the electron coupling matrix element connecting the initial fluorescing state ($S_1$) and the final charge transfer state (CT), and $\langle \rho_{FC} \rangle$ is the density of final vibronic states averaged over the separation in 0-0 transitions[9]. $\langle \rho_{FC} \rangle$ can be expressed in terms of the energy difference, $\Delta E_{00}$ ($\Delta E_{00}$ is defined as the difference between the bottom of the

wells in figure 9), for the removal of an electron from the donor and the capture of an electron by the acceptor by the following equation:

$$\langle \rho_{FC} \rangle = \frac{1}{\sqrt{2\pi\sigma^2}} \int \rho_{FC}(\Delta E_{00}) e^{-\frac{1}{2}\left(\frac{\Delta E_{00} - \langle \Delta E_{00} \rangle}{\sigma}\right)^2} d\Delta E_{00} \qquad (3)$$

where σ is the standard deviation of the $\Delta E_{00}$ about $\langle \Delta E_{00} \rangle$.

The formalism from Eqns. 1-2 to Eqn. 3 was first treated by Levich and Dogonadze, in which it was recognized that non-adiabatic electron transfer was a

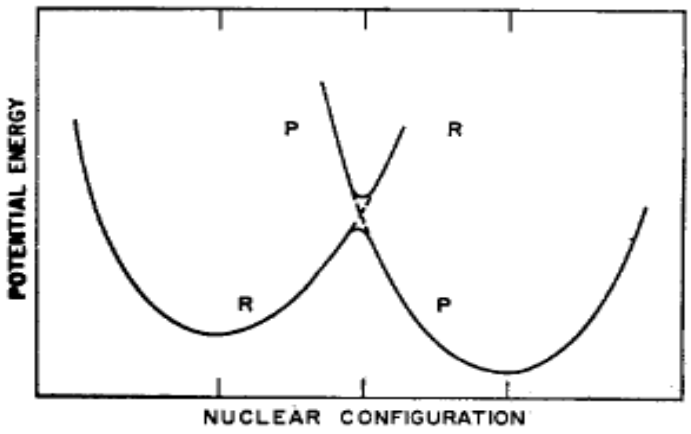


Figure9[10]: Plot of the Gibbs free energy (not potential energy) surface of Reactants (R) and Products (P) versus the nuclear configuration of all the atoms. The dotted lines refer to the system having zero interaction (non-adiabatic) and the solid lines refer to the adiabatic limit.

radiationless electronic transition[38-40].

Given this, the fluorescence quantum yield $\left(\frac{\text{photons emitted}}{\text{photons absorbed}}\right)$ is calculated as the ratio of rates of transition, as illustrated by Eqn. 4:

$$\Phi_{fl} = \frac{k_{rad}}{k_{nr} + k_{rad} + k_{ET}} \qquad (4)$$

where $k_{nr}$ is the sum of all the nonradiative (non-ET) decay rates, $k_{rad}$ is the radiative decay rate (fluorescence rate), and $k_{ET}$ is the ET rate (non-radiative). The fluorescence lifetime is:

$$\tau_{fl} = (k_{rad} + k_{nr} + k_{ET})^{-1} \tag{5}$$

Assuming $k_{nr}$ and $k_{rad}$ are constant regardless of the presence of a quencher, $k_{ET}$ becomes the only variable in $\Phi_{fl}$ and $\tau_{fl}$ variability.

The true rate is defined by equation 1, where the instantaneous rate constant is a function of both the interaction and the density of final states. In this manner we can define the average rate constant as:

$$\langle k_{ET} \rangle = 4\pi^2 c \langle V^2 \rho_{FC} \rangle \tag{6}$$

where the rate is calculated at every point and then averaged.

However, if the interaction and the density of states are not correlated, then the average rate constant can be written as:

$$\langle k_{ET} \rangle = 4\pi^2 c \langle V^2 \rangle \langle \rho_{FC} \rangle \tag{7}$$

where the average density of states and the average interaction are used to calculate the rate. If V and $\rho_{FC}$ are uncorrelated equations 6 and 7 should be equivalent.

If, as the Xie group assumes, the process is activationless, then equation 6 is used but the energy gap is adjusted so that the calculated $<\Delta E_{00}>$ corresponds to the maximum density of states and can be written as:

$$\langle k_{ET} \rangle_{Max} = 4\pi^2 c \langle V^2 \rho_{FC,0} \rangle \tag{8}$$

# RESULTS

## Flavin reductase (1QFJ)

### The Role of the $E_{00}$ Separation

Previous fluorescence trajectories done on Fre-Rbf and Fre-FMN were completed by Callis and Liu[6]. They rationalized that Rbf would be quenched better than FMN because ET activation energy (CT-$S_1$ energy gap) was smaller for Rbf (Figure 11). The higher activation energy for FMN was concluded to be due to the -2 charge from the phosphate group, which is missing in the Rbf case, and that the electron transfer is moving in the direction of the phosphate (Figure 10). Given this, it would be expected that the activation energy of Fre-FAD electron transfer would be similar to that of Fre-FMN (same -2 charge on the phosphate group). However, trajectories run by Callis et al. and duplicated for this work show that the CT-$S_1$ energy gap is closer to that of Fre-Rbf (Figure 11). This seems counter intuitive at first, but given a cumulative effect from the local potential environment, the CT state of the FAD is significantly lower than that

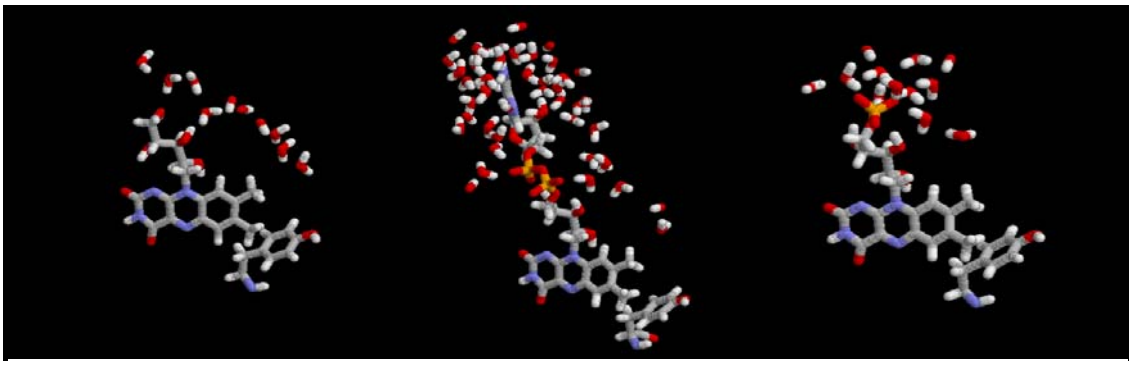

Figure 10: Images of Fre-Rbf (left), Fre-FAD (middle), and Fre-FMN (right). All show the location of the nearest Tyr and the extent of hydration of the flavin and the direction of electron transfer.

of the FMN.

Also, it is noteworthy that none of the trajectories are identical. This is of interest because it suggests that the ET in the Fre-flavin system cannot be an activationless process. At least two must have an activation barrier, contrary to what Xie et al.[20] reports.

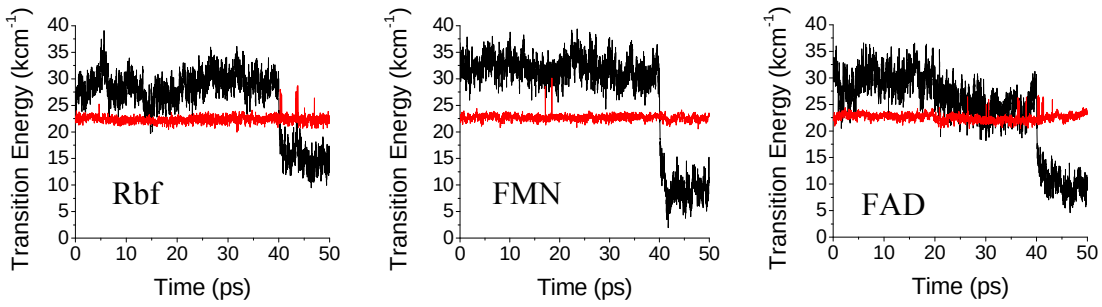


Figure 11: Trajectories of the 3 flavin-tyr pairs in 1QFJ. Plot of CT (black) and $S_1$ (red) transition energies ($kcm^{-1}$) vs. time (ps).

Electrostatic Sontrol of the Energy Gap

The differences between the structures of Fre-FAD, Fre-FMN, and Fre-Rbf are small and initially they appear identical. In fact, it would be easy to assume that the -2 charge on FMN and FAD would cause an equally large increase in the CT-$S_1$ energy gap. While this -2 charge does cause a large increase relative to Rbf, there are other

Table 1: Average coulombic stabilization (CS) has a big effect on the energy CT-$S_1$ energy gap. This effect is demonstrated by the table above.

| | **Energy Gap ($cm^{-1}$)** | **CS flavin ($cm^{-1}$)** | **CS Asp227 (cm-1)** | **Tyr35-Asp227 distance (Å)** | **CS Glu94 (cm-1)** | **Tyr35-Glu94 distance (Å)** |
|---|---|---|---|---|---|---|
| **FAD** | 4300 | 2300 | -8800 | 3.04 | -3900 | 3.70 |
| **FMN** | 8600 | 1600 | -8400 | 4.11 | -3300 | 4.43 |
| **Rbf** | 5400 | -3700 | -7900 | 3.79 | -4000 | 4.24 |

mitigating factors that also bring the FAD back down and not the FMN.

Small movements in the binding pocket, to accommodate the larger FAD, are the cause of the decrease in the energy gap. Two of the major residues responsible for "pushing" the electron from Tyr35 to the flavin, Asp227 and Glu94, are closer to the Tyr by about an angstrom in the case of FAD than with the FMN (Table 2R). With those two negative residues closer, about 1500 $cm^{-1}$ worth in coulombic stabilization can be accounted for (Table 1).\

CI Hamiltonian Matrix Element

The role of the electronic coupling between the fluorescing state and the charge transfer rate is of interest because of the high value that Xie et al[20] has placed on it as a controlling factor of the electron transfer rate. By using MO densities, calculated by Gaussian, we can identify the HOMO and LUMO for both the flavin and the residue (Figure 12). Once the HOMO and LUMO for each molecule are identified, the interaction between fluoresing state and the CT state can be calculated using the CI matrix.

As expected the average interaction depends exponentially on the distance between the CT pair (Figure 13). While there are many different orientations that the pair can sample at each distance, the average orientation at every distance should be similar.

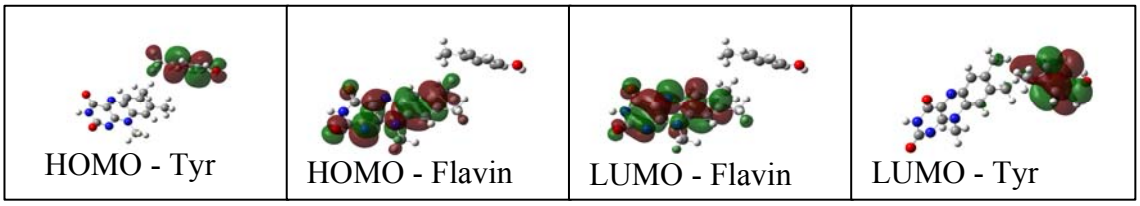


Figure 12: MO surfaces for the flavin/tyr CT pair. Shown in order of increasing energy level.

This is seen in our calculations and offers validity to our method. Since the interaction (V) in very sensitive to distance and orientation, it can be expected that it would vary greatly over the course of the dynamics. In fact what is seen is V varies from near zero to $10^3$ $cm^{-1}$. While there is a strong distance dependence of the interaction, as shown by Figure 13, this does not account for the rapid fluctionations in V in as little as 10 fs. This can be explained by the fact that the interaction is proportional the overlap of the initial and final configurations. This means that while the distance between the flavin and the Tyr will not change as rapidly as the V, the change in overlap will. This is caused by small lateral movements between the pair.

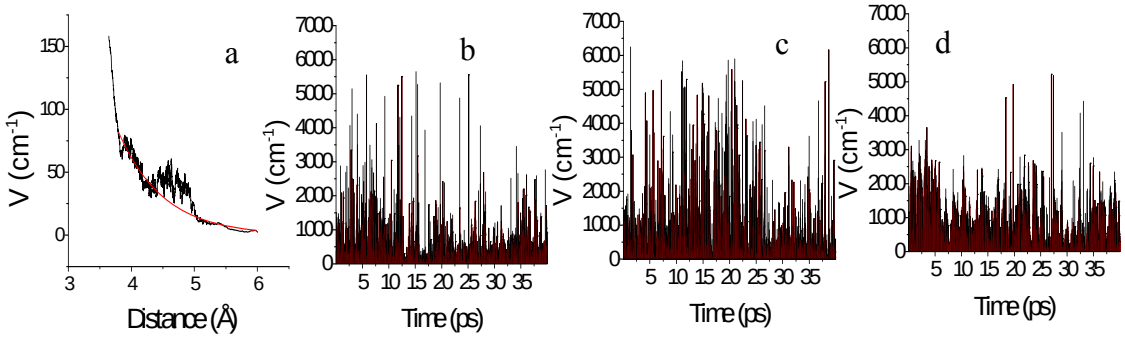


Figure 13: Calculation of |V| as a function of (a) distance (Å) and of (b-d) time (ps) for the three flavins. FAD (b), FMN (c), and Rbf (d).

Electron Transfer Rate ($k_{ET}$) and the Quantum Yield ($\Phi_{fl}$)

The impact of both the interaction and the energy gap are profound, as can be seen by Figure 14. The change in energy gap and the interaction, in as little as 10 fs, is astounding. Given this rapid change in both components, it is no surprise that the rate

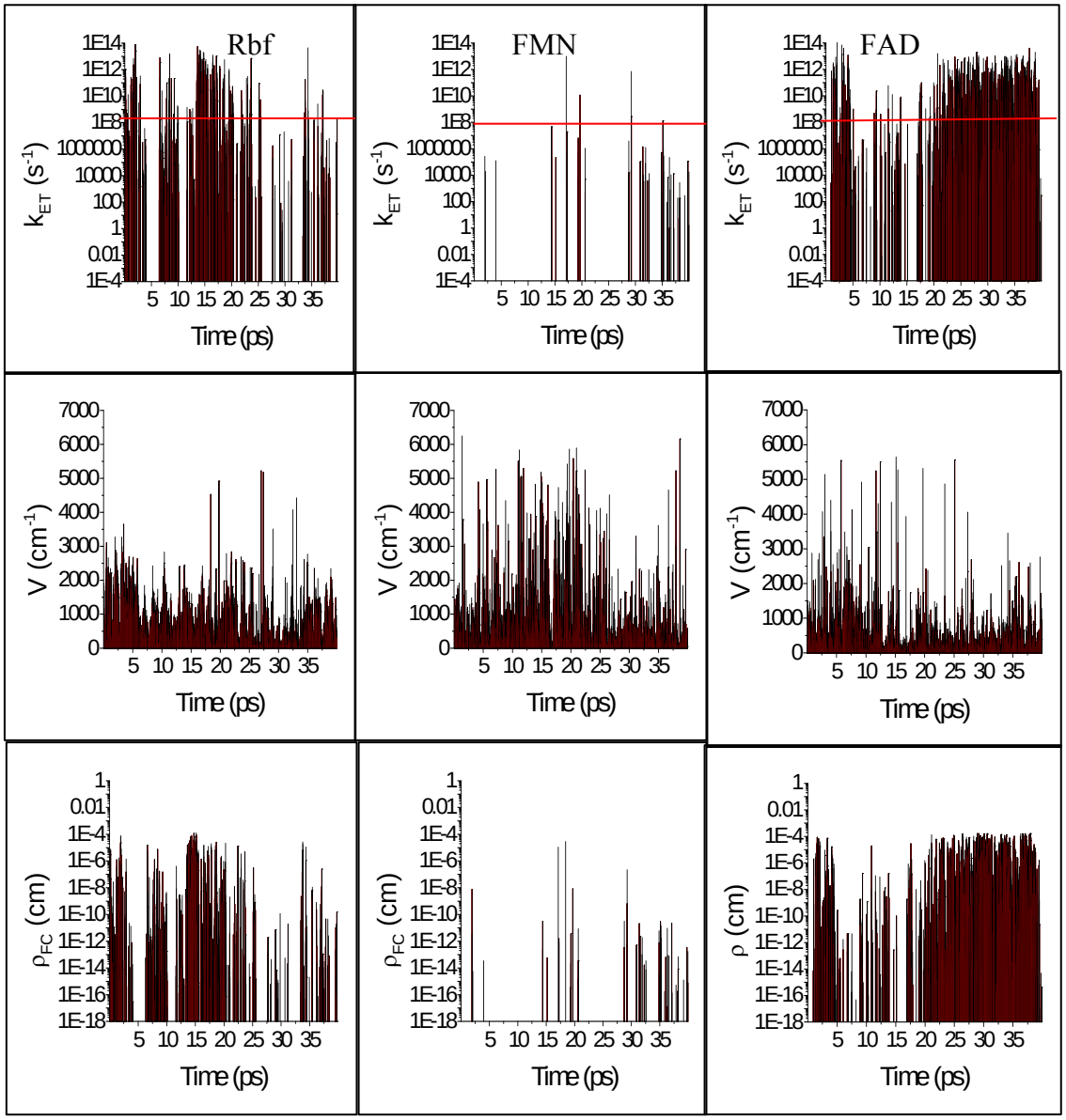


Figure 14: Relationship between the instantaneous rate, interaction and $\rho_{FC}$ (density of states). Red line shows the approximate location of the radiative and nonradiative rates.

changes just as rapidly with time. However, it is apparent that the instantaneous rate is only non-zero some of the time. Even in the case of FAD and Rbf, the rate constant appears to be zero or significantly low (as compared to the radiative rate) most of the time. This suggests that the electron transfer event only occurs when the dye and residue have the appropriate arrangement. Also, there does seem to be a large correlation between the density of states and the rate, whereas that correlation does not seem to exist for the interaction and the rate. This can be seen in that when the density of states is low, so is the rate and vice versa.

As can be seen by table 2, the rate is drastically different depending on what method is used for the calculation. Since calculating the rate at every point and then averaging all the rates ($<V^2\rho_{fc}>$) is the most appropriate method (no assumptions about

Table 2: Average kET ( $s^{-1}$) is calculated three different ways for the three flavins.

| | $< V^2\rho_{fc}>$ | $<V^2><\rho_{fc}>$ | $< V^2\rho_{fc,0}>$ |
|---|---|---|---|
| Rbf | $1.84 \times 10^{11}$ | $1.75 \times 10^{11}$ | $2.36 \times 10^{13}$ |
| FMN | $2.59 \times 10^{9}$ | $3.41 \times 10^{9}$ | $2.47 \times 10^{12}$ |
| FAD | $2.32 \times 10^{11}$ | $3.16 \times 10^{11}$ | $2.31 \times 10^{13}$ |

Table 3: The average calculated $k_{ET}$ is related to the measured $k_{rad}$ and $k_{nr}$. The calculated quantum yield and lifetime is compared to measured value of $\tau \approx 0.5$ns for FAD and FMN.

| | $k_{ET}$ ($s^{-1}$) | $k_{rad}$ ($s^{-1}$) [25] meas | $k_{nr}$ ($s^{-1}$) [25] meas | $\Phi_{fl,free}$ meas | $\Phi_{fl,bound}$ | $\tau_{fl,free}$ (ps) meas | $\tau_{fl,bd}$ (ps) |
|---|---|---|---|---|---|---|---|
| Rbf | $1.84 \times 10^{11}$ | $6.67 \times 10^{7}$ | $1.56 \times 10^{8}$ | 0.30 | $3.6 \times 10^{-4}$ | 4500 | 5.5 |
| FMN | $2.59 \times 10^{9}$ | $6.34 \times 10^{7}$ | $1.80 \times 10^{8}$ | 0.26 | 0.02 | 4100 | 350 |
| FAD | $2.32 \times 10^{11}$ | $6.45 \times 10^{7}$ | $2.58 \times 10^{8}$ | 0.20 | $2.8 \times 10^{-4}$ | 3100 | 4.3 |

the energy gap and interaction fluctuations), we can assume it to be the best approximation of the true average rate constant.

Table 2 shows that when the average energy gap is adjusted to maximize the density of states, the ET rate is far too fast, and gives lifetimes on the order of 100 fs and not 500 ps as is measured by Xie et al[20]. This indicates that the quenching is not

Table 4: Comparison of Vrms, $<\rho_{FC}>$, $\sigma_{\Delta Eoo}$, and $<E_{00}>$ for the three flavins.

| | $V_{rms}$ ($cm^{-1}$) | $<\rho_{FC}>$ (cm) | $\sigma_{\Delta Eoo}$ ($cm^{-1}$) | $<\Delta E_{00}>$ ($cm^{-1}$) |
|---|---|---|---|---|
| Rbf | 930 | $2.0 \times 10^{-7}$ | 2400 | 4300 |
| FMN | 1021 | $3.4 \times 10^{-9}$ | 2200 | 8600 |
| FAD | 690 | $5.0 \times 10^{-7}$ | 3300 | 5400 |

Table 5: The fractional standard deviation of $V^2$, $\rho_{FC}$, $k_{ET}$ for the three flavins. Also the range of lifetimes calculated.

| | $\sigma_V 2$ | $\sigma_\rho$ | $\sigma_{kET}$ | Lifetime range (ns) |
|---|---|---|---|---|
| Rbf | 2.00 | 12.01 | 17.09 | 0.002 – 4.5 |
| FMN | 3.22 | 54.38 | 55.49 | 0.13 – 4.1 |
| FAD | 3.86 | 3.75 | 9.55 | 0.003 – 3.1 |

activationless but does indeed have an energy barrier. The second point that can be made is that the fluctuations in the energy gap are large (10~20kT) and do cause large fluctuations in the observed rate as can be seen by Tables 4 and 5. In fact, the fractional deviation (standard deviation/average) of the density of states is 6-20 times larger than that of the interaction (Table 5). This is a clear indication that the energy gap fluctuations and not the change in the interaction (distance or orientational) has a majority control over the rate, this is with the exception of the FAD case where the

fluctuations in the interaction and the density of states appear to make equal contributions.

With the average electron transfer rate calculated, an approximation of the fluorescence quantum yield and the effective lifetime can be made. Table 3 shows that the calculated quantum yields and lifetimes are similar to those measured by Xie (even if the estimations are a little low for Rbf and FAD). Another result measured by Xie, is the range of lifetimes measured for each of the flavins (30 ps – 3 ns). As can be seen in Table 5, the range of lifetimes calculated are similar to those measured.

## Anti-Fluorescein (1FLR)

### The Role of the $E_{00}$ Separation

The interest in the fluorescein antibody was, also inspired by the Xie group[21]. Looking at the crystal structure of 1FLR (figure 15), it is easy to notice the 4 Tyrs and 2 Trps that are within 5-10 Å of the fluorescein. From this alone it seems hard to say definitively

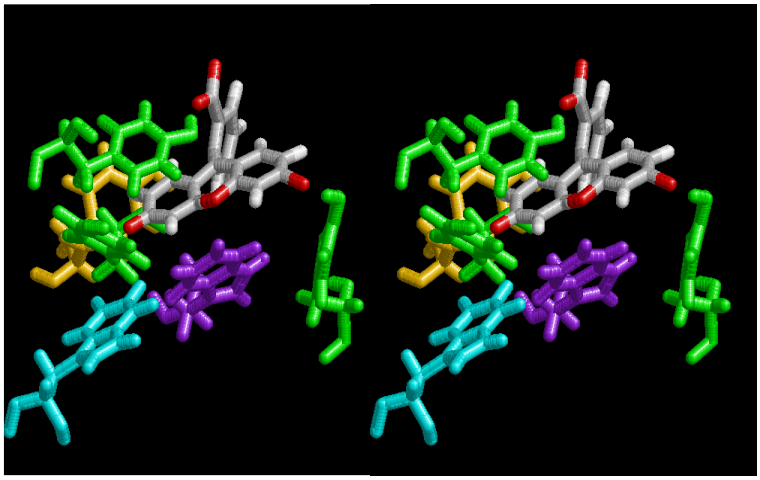

Figure 15: Position of six potential quenchers around fluorescein.

which residue is quenching or whether it is only one, especially in light of Mataga's sandwiched flavins).

In order to compute the transition energies of the CT and $S_1$ states, a new topology file was created for fluorescein in the ground state and with a -2 charge. This was done because fluorescein is most fluorescent in the dianion form. Furthermore, the Xie and coworkers[21] studies were done at physiological pH, and it was assumed that the dominant species was the dianion.

With the new topology file, QM-MM simulations were run, in the hope of distinguishing between the six candidates. As can be seen by figure 16 none of the 6 possible quenchers had a low energy gap, unlike the case with Fre-Rbf and Fre-FAD where the CT state occasionally fell below that of the $S_1$ state. It is noted that even

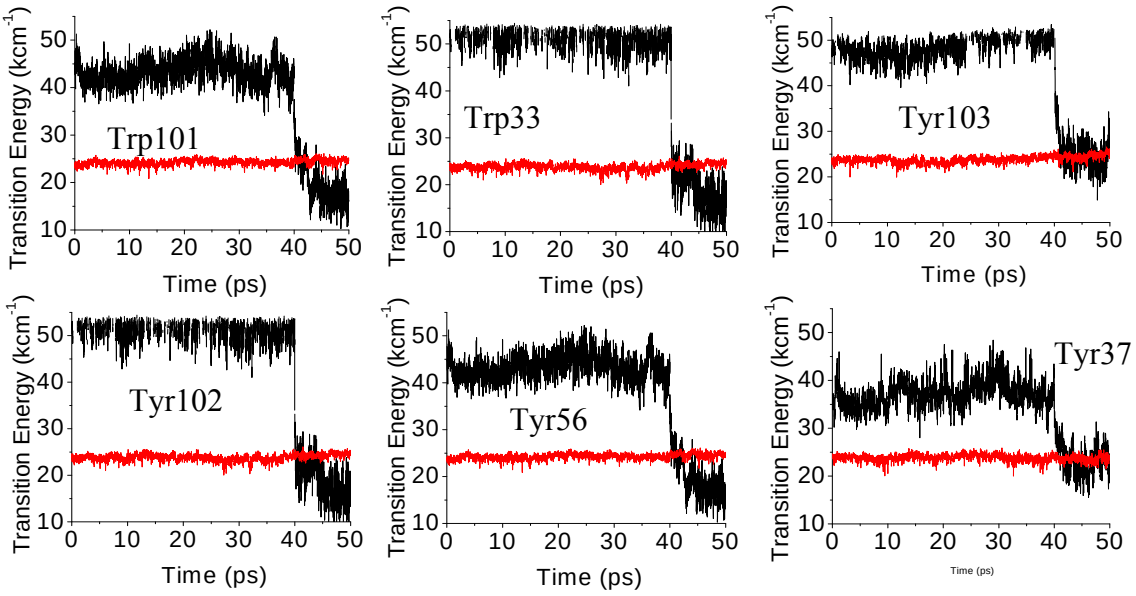


Figure 16: Trajectories of the 6 possible quenchers of fluorescein in 1FLR. Plot of CT (black) and $S_1$ (red) transition energies ($kcm^{-1}$) vs. time (ps).

though none of the residues has a low energy gap, Tyr56 and Tyr37 both have significantly lower energy gaps than the rest. This would suggest that the two most likely to quench would be one of those two. However, in the absence of knowledge of the interaction, not even Tyr56 and Tyr37 can be considered as great candidates for quenching.

This is surprising considering that studies have shown Trp to be a better quencher than Tyr (both with flavins and fluorescein)[20-21] due to a higher lying HOMO for the Trp than the Tyr. Given this, the opposite would be expected, especially since the closest Trp is within van der Waals contact of the xanthene ring.

Electrostatic Control of the Energy Gap

| **Residue** | **Tyr37** | **Tyr56** | **Tyr102** | **Tyr103** | **Trp101** | **Trp33** |
|---|---|---|---|---|---|---|
| **Edge to edge distance (Å)** | 3.50 | 4.10 | 7 | 3.64 | 4.01 | 3.65 |
| **Average $\Delta E_{00}$ ($cm^{-1}$)** | 13200 | 19150 | 27100 | 24300 | 20700 | 22850 |
| **ES (benzoate) ($cm^{-1}$)** | -4320 | 3219 | 8018 | 3778 | 9420 | 8152 |

Table 6: The impact of the distance and the electrostatic (ES) effect of the negative charge on the benzoate moiety of the fluorescein on the average energy gap.

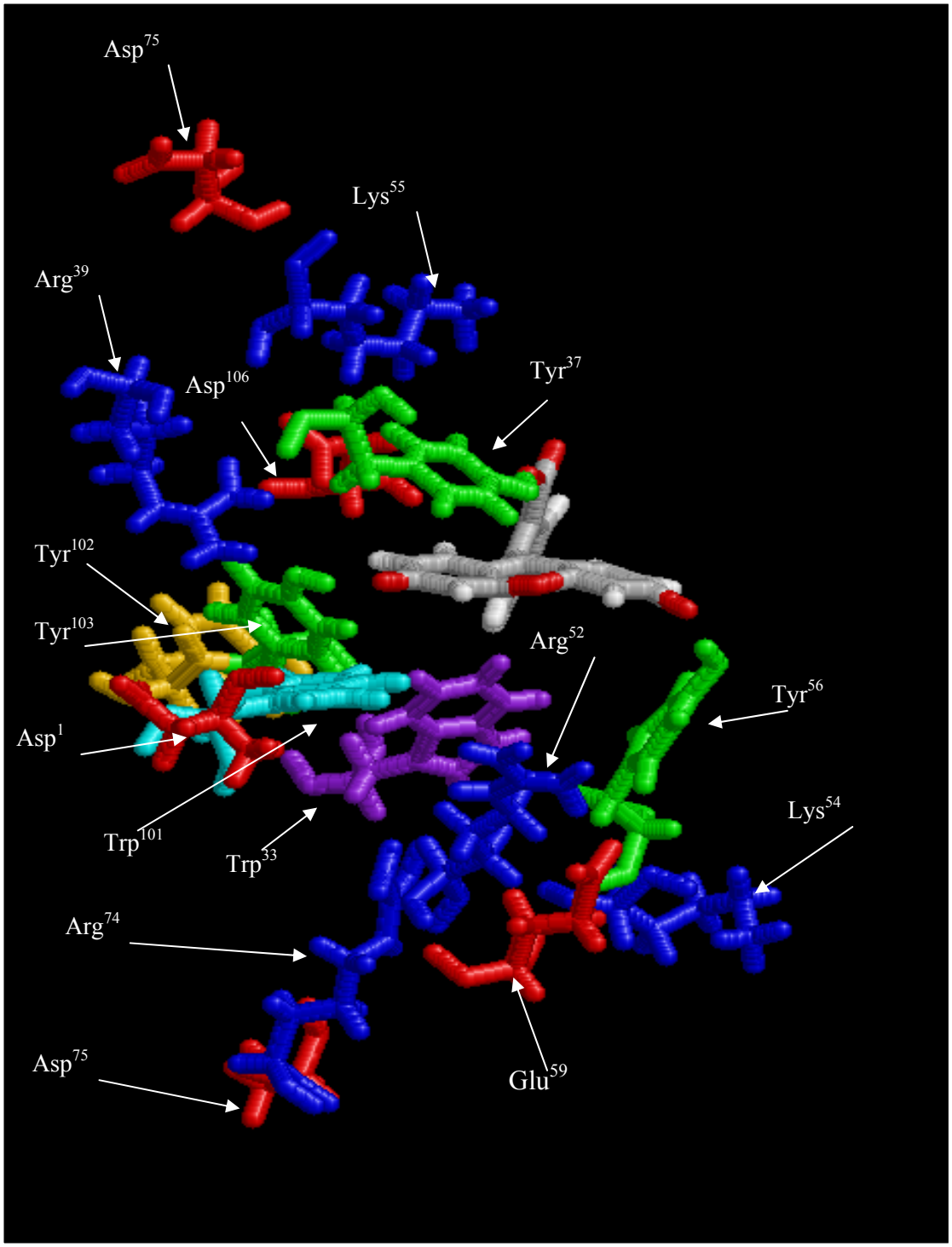


Figure 17: Picture of the fluorescein binding pocket with the six possible quenchers and several important charged residues. Positively charged residues are blue and negatively charged residues are red.

As in the case of the flavin, to better understand this, a close look at the

coulombic stabilization/destabilization of each residue is warranted. Given the fact that the two closest Tyr have a lower $\Delta E_{00}$ than that of the closest Trp (Table 6), there must be a stabilizing force present for the Tyr's and not the Trp's. By using Coulomb's Law an estimation of the effect of the local electric field on the electron transfer can be made. This impact can be seen in Table 6. Since the electron transfers from the residues to the xanthene ring on the fluorescein, one of the biggest contributors to the stabilization or destabilization of the CT state will be the negative charge on the benzoate moiety on the fluorescein itself. In every case, save the Tyr37, the electron is being transferred toward this negative charge (Figure 15). In the case of Tyr37, not only is the transfer occurring away from the negative charge, the resulting positive charge on the phenyl ring of the Tyr only polarizes the OH bond more and thereby strengthening the hydrogen bond between the Tyr and the benzoate group on the fluorescein. This in turn holds the ET pair together and stabilizes the CT state, while the other residues are relatively free to move to and from the fluorescein.

While the benzoate group on the fluorescein certainly has a very large effect, and

Table 7: Average coulombic stabilization (CS) has a big effect on the energy CT-S1 energy gap. This effect is demonstrated by the table above. Highlighted values are residues of interest.

| | **Energy Gap ($cm^{-1}$)** | **CS Arg39 ($cm^{-1}$)** | **CS Arg52 ($cm^{-1}$)** | **CS Arg74 ($cm^{-1}$)** | **CS Asp1 ($cm^{-1}$)** | **CS Asp106 ($cm^{-1}$)** | **Total CS ($cm^{-1}$)** |
|---|---|---|---|---|---|---|---|
| **Tyr37** | 13200 | **2700** | 820 | 750 | 400 | **-6000** | -1330 |
| **Tyr56** | 19150 | -1600 | **9850** | **4650** | -15 | **2850** | 15735 |
| **Tyr102** | 27100 | -1250 | -1900 | **6569** | -250 | **4200** | 7369 |
| **Tyr103** | 24300 | **7750** | **3000** | **4850** | -200 | **-2850** | 12750 |
| **Trp33** | 22850 | 2100 | **13350** | **8900** | -250 | 700 | 24800 |
| **Trp101** | 20700 | **10150** | 1650 | 2300 | **-600** | **-2850** | 10650 |

arguably the largest, there is one other factor that pushes the energy gap of the other residues higher relative to Tyr37.

This factor is the placement of charged residues around the fluorescein, specifically three arginines (Arg39, Arg52, and Arg74) and two aspartates (Asp1and Asp106). As can be seen by Figure 17 and Table 7, these residues have the effect of destabilizing the electron transfer from Tyr103, Trp33, and Trp101 (Asp1 has the opposite effect on Tyr101). Arg39, 52, and 74 are of particular interest because they are placed opposite the direction of the electron transfer, and thereby destabilize the electron transfer from the Trp's. Asp106 is another residue of interest because its placement helps drive the electron transfer from Tyr37 to the fluorescein.

The net effect of these five residues is a destabilization of all but the CT state of the Tyr37-Flu pair. While the stabilization of Tyr37 is minimal, the destabilization of the others is drastic, especially Trp33. In fact, there is good correlation between the coulombic stabilization energy and the $S_1$-CT energy gap. The notable exception being Tyr102, but this can be explained by the fact that it is father away from the fluorescein, by a couple of angstroms, than any of the other candidates. This exception is notable because even with the coulombic stabilization, the energy gap remains high because of the large distance between the Tyr and fluorescein.

CI Hamiltonian Matrix Element

The case for anti-fluorescein is a bit more complicated than for flavin, in that the

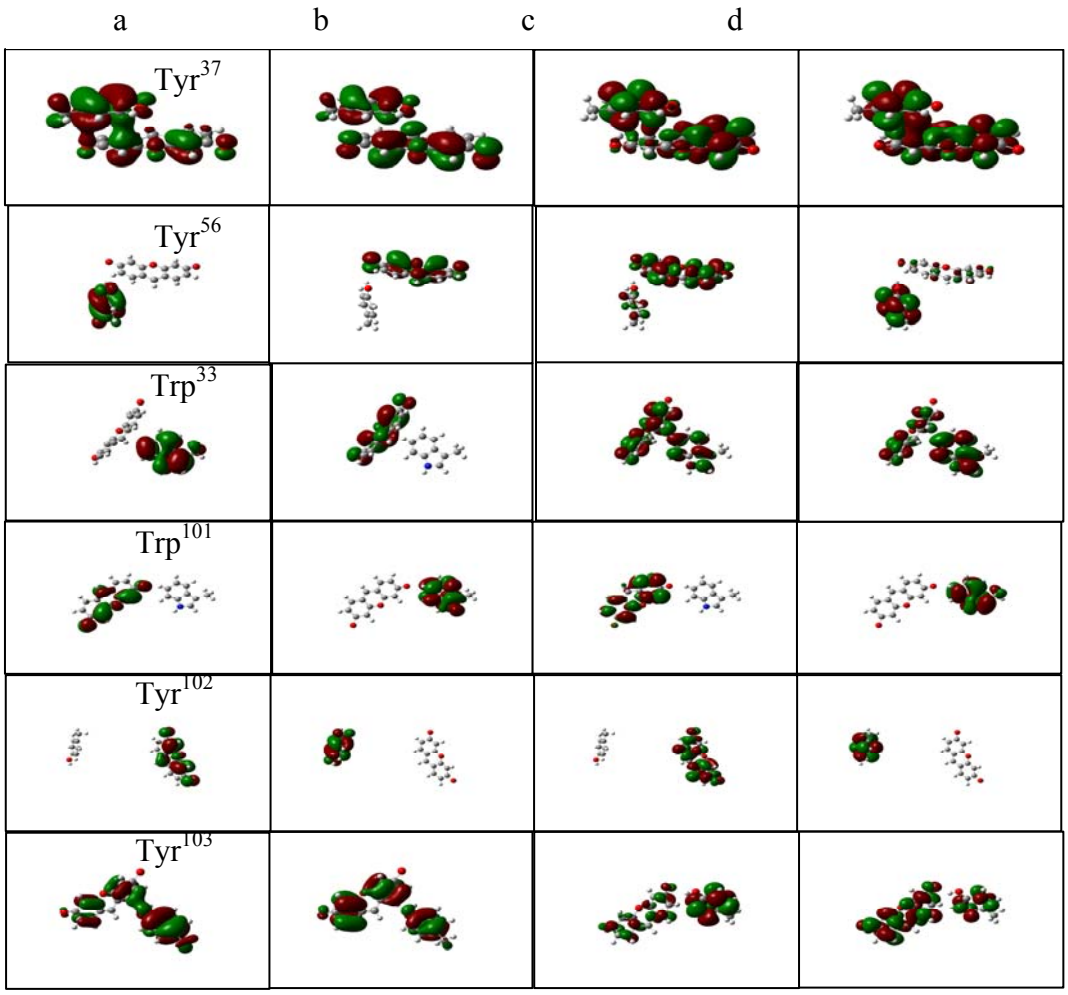


Figure 18: Mixing between the residue HOMO (a) with the HOMO – n (b) of fluorescein and/or the LUMO (c) of the residue with the LUMO + n (d) of fluorescein of the six residues. MO's are listed in order of energy (right to left).

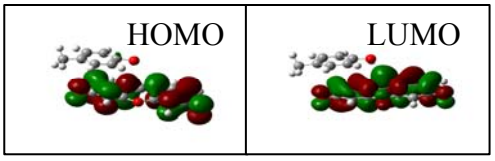


Figure 19: Representation of the HOMO and LUMO of fluorescein.

HOMO and LUMO for the residue generally are not pure. There is a great deal of mixing between the LUMO of the residue and the LUMO + n of fluorescein and the HOMO of the residue and the HOMO - n of the fluorescein (figure 18). Therefore a linear combination of the molecular orbital coefficients was taken in order to maximize the content on the residue. The interaction was then taken as a partial sum of two interactions based on the residue content.

As can be seen by figure 20, the V varies from zero to a few hundred to nearly 1000 $cm^{-1}$ depending on the residue . This is with the exception of Tyr102 which never has a significant interaction with the fluorescein. While the exponential decay of the interaction with respect to distance is witnessed in all of the residues, there are a couple of notable exceptions. Tyr37 and Tyr56 display non exponential behavior inside of 3 Å,

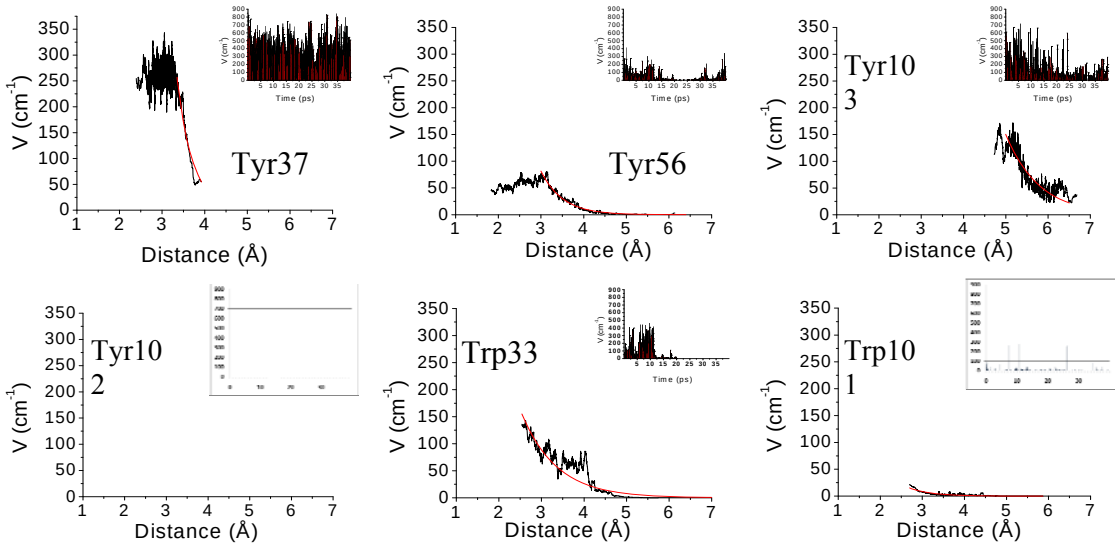


Figure 20: Distance dependence of the average interaction. Created by binning 50 consecutive interactions ($cm^{-1}$) and distances (Å) over the course of the trajectory after sorting by distance. Inset: Interactions as a function of time (ps).

this is likely due to orientational effects at such close distances as well as hydrogen bonding.

Electron Transfer Rate ($k_{ET}$) and the Quantum Yield ($\Phi_{fl}$)

As was the case with the flavin reductase, the change in energy gap, interaction and rate all change rapidly with time. Also, what can be seen from Figures 21 and 22 is that the rate does appear to correlate quite well with the fluctuations in the density of states and not much with the interaction. Another similarity is that the rate is nearly zero or significantly small a majority of the time. Meaning that the few events where the ET rate is larger than the radiative rate are what determine the quenching ability of the system. Once again, the system has to be in a specific orientation in order for the electron transfer event to occur.

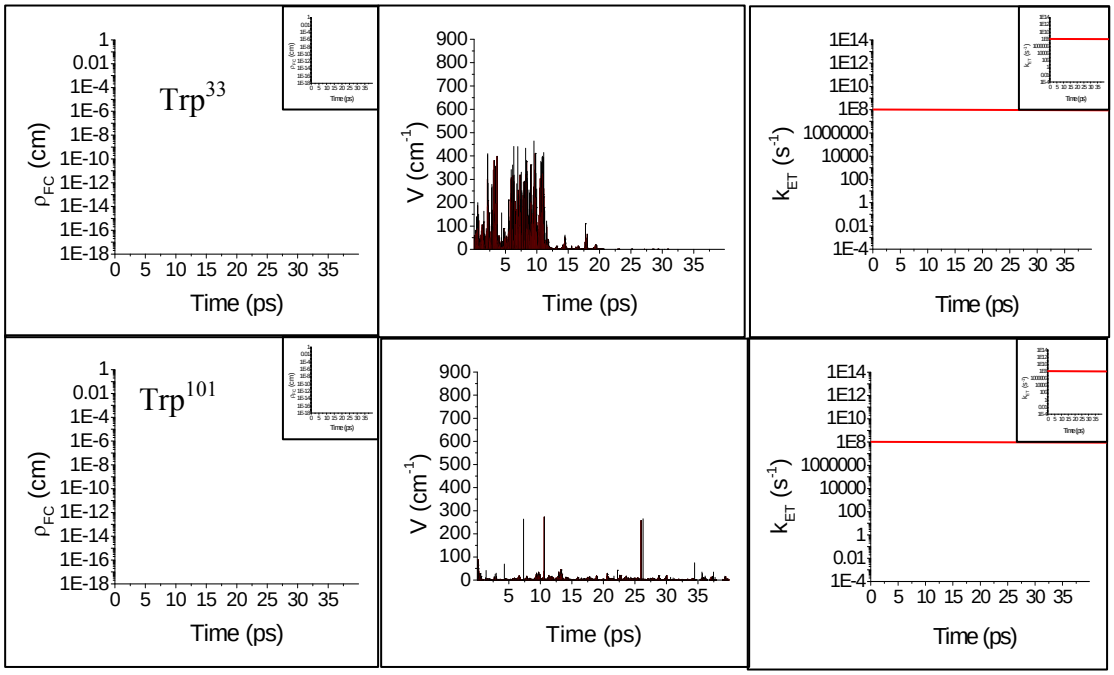


Figure 21: Relationship between the instantaneous rate (right) and interaction (middle) and energy gap (left) for the two Trps. Red line shows the approximate location of the radiative and nonradiative rates. Insets: The same relationship but without the energy gap correction.

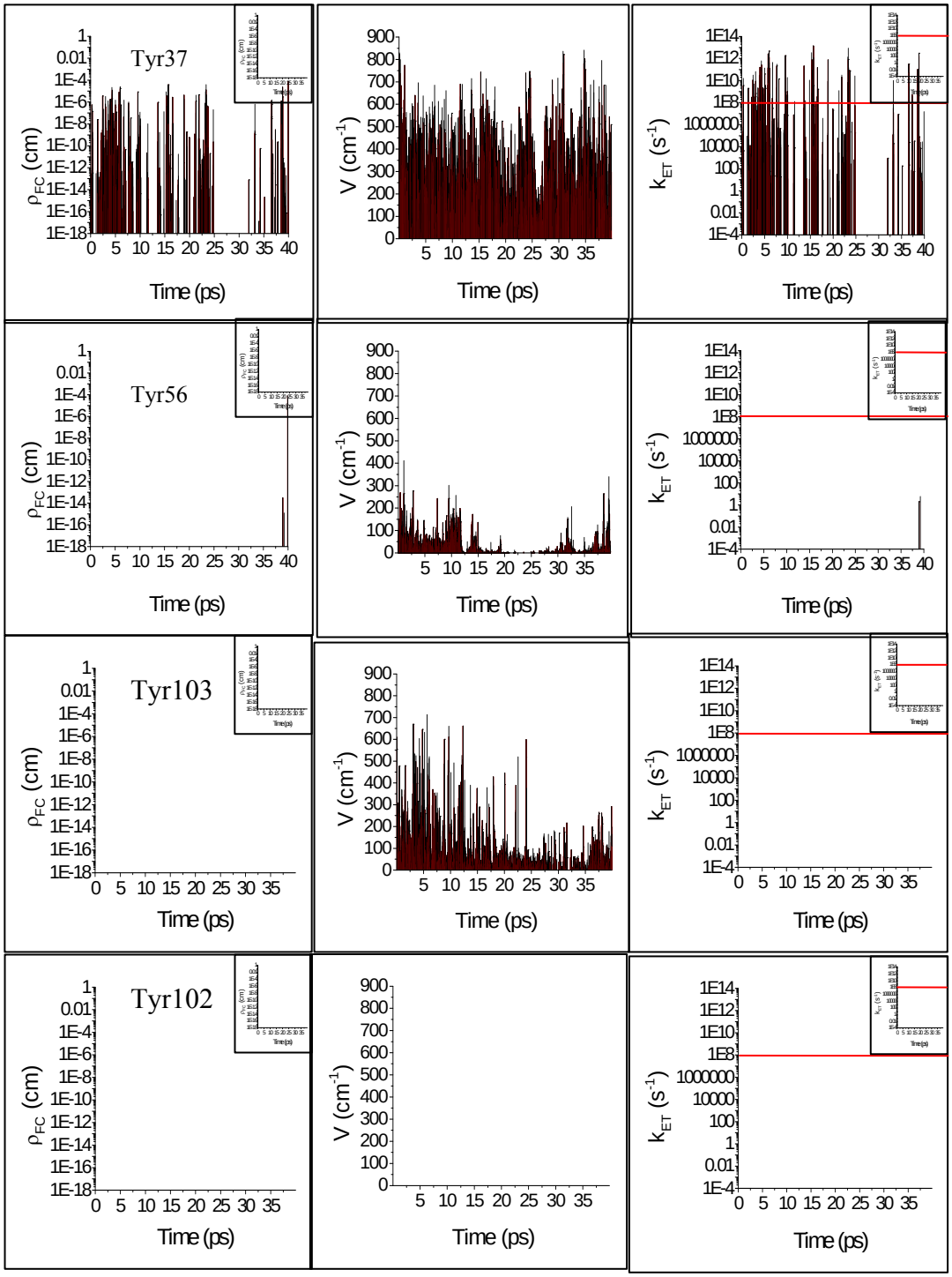


Figure 22: Relationship between the instantaneous rate (right) and interaction (middle) and energy gap (left) for the four Tyrs (37,56,103,and 102). Red line shows the approximate location of the radiative and nonradiative rates. Insets: The same relationship but without the energy gap reduction (same scale).

Table 8: The fractional standard deviation of $V^2$, $\rho_{FC}$, and kET for the six resides. Also shown is the calculated lifetime range

| | $\sigma_V 2$ | $\sigma_\rho$ | $\sigma_{kET}$ | Lifetime Range (ns) |
|---|---|---|---|---|
| $Tyr^{37}$ | 1.32 | 28.13 | 34.81 | 0.10 – 4.1 |
| $Tyr^{56}$ | 3.13 | ----- | ----- | ----- |
| $Tyr^{102}$ | ----- | ----- | ----- | ----- |
| $Tyr^{103}$ | 3.24 | ----- | ----- | ----- |
| $Trp^{33}$ | 4.43 | ----- | ----- | ----- |
| $Trp^{101}$ | 18.26 | ----- | ----- | ----- |

Table 9: Comparison of Vrms, $<\rho_{FC}>$, $\sigma_{\Delta Eoo}$, $<\Delta E_v>$, and $<\Delta E_{00}>$ for the six residues.

| | $V_{rms}$ ($cm^{-1}$) | $<\rho_{FC}>$ (cm) | $\sigma_{\Delta Eoo}$ (cm) | $<\Delta E_v>$ ($cm^{-1}$) | $<\Delta E_{00}>$ ($cm^{-1}$) |
|---|---|---|---|---|---|
| $Tyr^{37}$ | 304 | $1.8 \times 10^{-7}$ | 2600 | 13200 | 8100 |
| $Tyr^{56}$ | 54 | 0 | 2900 | 19150 | 14050 |
| $Tyr^{102}$ | 0 | 0 | 2100 | 27100 | 22100 |
| $Tyr^{103}$ | 115 | 0 | 2200 | 24300 | 19200 |
| $Trp^{33}$ | 62 | 0 | 2180 | 22850 | 17750 |
| $Trp^{101}$ | 11 | 0 | 2540 | 20700 | 15600 |

This is further demonstrated by the fact that the fraction deviation of $V^2$ is 10-20 times smaller than that of the density of states (Table 8). Also, Table 9 shows that the standard deviation of the energy gap is large (10-20kT). Given that the calculated energy gaps for all the residues were too high to calculate a rate and adjustment of -5100 $cm^{-1}$ was added to every gap. This correction lowered the energy gap for the Tyr37 enough to have a calculated lifetime of 520 ps. With this adjustment only the Tyr37 is shown to have a significant calculated rate.

This adjustment can be rationalized by the fact that the calculated absorption $\lambda_{max}$ for the fluorescein is 418 nm vs. the measured $\lambda_{max}$ of 495 nm. This blue shift in $\lambda_{max}$ is an indication that the method we use to calculate the transition energies is not completely

calibrated for large anionic systems. This is in contrast to the calculated $\lambda_{max}$ of 444 nm for the flavin (no adjustment needed), which is in good agreement with the experimental value of 450 nm (Photochem CAD).

Even with the adjustment made, the average density of states is still 2 – 3 orders of magnitude lower than if an activationless process is assumed (Table 10). Also, we can see that the rate is not activationless by the comparison of $< V^2\rho_{fc}>$ and $<V^2\rho_{fc,0}>$. As with the flavin, the overly large rate constant calculated by assuming that the average $\Delta E_{00}$ is activationless, is an indication that there is at least some activation energy required for quenching.

Table 10: Average kET ($s^{-1}$) calculated three different ways for the six residues, after an energy gap reduction of 5100 $cm^{-1}$.

| | $< V^2\rho_{fc}>$ | $< V^2\rho_{fc,0}>$ | $<V^2><\rho_{fc}>$ |
|---|---|---|---|
| Tyr37 | $1.69 \times 10^{9}$ | $5.86 \times 10^{11}$ | $7.13 \times 10^{8}$ |
| Tyr56 | 0 | $3.6 \times 10^{6}$ | 0 |
| Tyr102 | 0 | 0 | 0 |
| Tyr103 | 0 | 0 | 0 |
| Trp33 | 0 | 0 | 0 |
| Trp101 | 0 | 0 | 0 |

As before, if the calculated rate is higher than the radiative rate, then the fluorescence is quenched, if not then there is not quenching. As table 10 shows the only residue that shows an average rate above the radiative rate is that of Tyr37 and thereby is the most probable quencher. Adding to this is that Tyr37 is the only residue that produces a rate faster than the radiative during the entirety of the trajectories (Figures 21 and 22). The other residues, with the exception of Tyr56, in 50 ps, never produce an

electron transfer event, adding further to the likelihood that Tyr37 is the most probable quencher.

# CONCLUSION

The application of a method previously developed by Callis et al to predict the quantum yields of Trp fluorescence has been successfully applied to the fluorescence of dyes and cofactors in proteins. While an adjustment was needed to empirically fit the measured lifetime of the fluorescein, our calculations were able to show similar fluctuations in the lifetime as those measured by Xie in both the Fre-Flavin and Anti-fluorescein cases.

Also shown is the ability to separate the interaction and activation energy components of the rate constant. From this separation, it was shown that the size and fluctuations of the energy gap do play a major role in the fluctuations in the rate constant. While it is true that the interaction plays a significant role, the energy gap can now be said have a larger impact on the lifetime variability. It was also shown that the electrostatic environment surrounding the fluorescent molecule plays a decisive role in modulating the fluctuations in the fluorescence lifetime. This was especially apparent in the fluorescein case, where the closest Tyr was determined to be the sole quencher. This was despite the fact that a Trp, which is a better quencher in aqueous media, was almost as close to the fluorescein. The electrostatics were shown to hinder the electron transfer from all the potential quenchers except the closest Tyr.

REFERENCES CITED

1. Eftink, M. R., *Methods Biochem. Anal.* 1991, 35, 127-205.
2. Meech, S. R.; Phillips, D.; Anthony, G., *Chem. Phys.* 1983, 80, 317-328.
3. Beratan, D. N.; Betts, J. N.; Onuchic, J. N., *Science* 1991, 252, 1285-1288.
4. Gray, H. B.; Winkler, J. R., *Annu. Rev. Biochem.* 1996, 65, 537-561.
5. Beratan, D. N., Betts, J. N., Onuchic, J. N., *J. Phys. Chem.* 1992, 96, 2852-2955.
6. Callis, P. R.; Liu, T., *Chem. Phys.* 2006, 326, 230-239.
7. Callis, P. R.; Liu, T., *J. Phys. Chem. B* 2004, 108, 4248-4259.
8. Liu, T.; Callis, P. R.; Hesp, B. H.; de Groot, M.; Buma, W. J.; Broos, J. , *J. Am. Chem. Soc.* 2005, 127, 4104-4113.
9. Callis, P. R.; Vivian, J. T., *Chem. Phys. Lett.* 2003, 369, 409-414.
10. Marcus, R. A., *J. Chem. Phys.* 1956, 24, 966-978.
11. Yu, H. T.; Colucci, W. J.; McLaughlin, M. L.; Barkley, M. D., *J. Am. Chem.* Eftink, M. R.; Jia, J.; Hu, D.; Ghiron, C. A., *J. Phys. Chem.* 1995, 99, 5713-5723.
12. Broos, J.; Maddalena, F.; Hesp, B. H. *J. Am. Chem. Soc.* 2004, *126*, 22-23.
13. Mataga, N.; Chosrowjan, H.; Shibata, Y.; Tanaka, F., *J. Phys. Chem. B*, 1998, 102, 7081-7084.
14. Mataga, N.; Chosrowjan, H.; Shibata, Y.; Tanaka, F.; Nishina, Y.; Shiga, K., *Phys. Chem. B* 2000, 104, 10667-10677.
15. Mataga, N.; Chosrowjan, H.; Taniguchi, S.; Tanaka, F.; Kido, N.; Kitamura, M., *J. Phys. Chem. B* 2002, 106, 8917-8920.
16. Mataga, N.; Chosrowjan, H.; Taniguchi, S., *J.Photochem. Photobiol.C* 2004, 5 155-168.

17. van den Berg, P. A. W.; van Hoek, A.; Walentas, C. D.; Perham, R. N.; Visser, A. J. W. G., *Biophys. J.* 1998, 74, 2046-2058.

18. van den Berg, P. A. W.; van Hoek, A.; Visser, A. J. W. G., *Biophys. J*. 2004, 87, 2577-2586.

19. Xie, X. S.; Trautman, J. K., *Annu. Rev. Phys. Chem.* 1998, 49, 441.

20. Yang, H.; Lou, G.; Karnchanaphanurach, P.; Louie, T.; Rech, I.; Cova, S.; Xun, L.; Xie, X. S., *Science* 2003, 302, 262-266.

21. Min, W.; Lou, G.; Cherayil, B. J.; Kou, S. C.; Xie, X. S., *Phys. Rev. Let.* 2005, 94, 198302.

22. Watt, R. M.; Voss, E. W., Jr., *Immunochem.* 1977, 14, 533-541.

23. Togashi, D. M.; Szczupak, B.; Ryder, A. G.; Calvet, A.; O'Loughlin, M., *J. Phys. Chem A* 2009, 113, 2757-2767.

24. Sjöback, R.; Nygren, J.; Kubista, M., *Spectrochemica Acta A* 1995, 51, L7-L21.

25. Miura, T.; Urano, Y.; Tanaka, K.; Nagano, T.; Ohkubo, K.; Fukuzumi, S., *J. Am. Chem. Soc.* 2003, 125, 8666-8671.

26. Ueno, T.; Urano, Y.; Setsukinai, K; Takakusa, H.; Kojima, H.; Kikuchi, K.; Ohkubo, K.; Shinichi, N.; Nagano, T., *J. Am. Chem. Soc.* 2004, 126, 14079-14085.

27. Lou, G.; Andricioaei, I.; Xie, X. S., *J. Phys. Chem. B* 2006, 110, 9363-9367.

28. Short, K. W.; Callis, P. R., *J. Chem. Phys*. 1998, 108, 10189-10196.

29. Theiste, D.; Callis, P. R.; Woody, R. W., *J. Am. Chem. Soc.* 1991, 113, 3260-3267.

30. Sreerama, N.; Woody, R. W.; Callis, P. R., *J. Phys. Chem.* 1994, 98, 10397-10407.

31. MacKerell, A. D.; Bashford, D.; Bellott, M.; Dunbrack, R. L.; Evanseck, J. D.; Field, M. J.; Fischer, S.; Gao, J.; Guo, H.; Ha, S.; Joseph-McCarthy, D.; Kuchnir, L.; Kuczera, K.; Lau, F. T. K.; Mattos, C.; Michnick, S.; Ngo, T.; Nguyen, D. T.; Prodhom, B.; Reiher, W. E., III; Roux, B.; Schlenkrich, M.; Smith, J. C.; Stote, R.; Straub, J.; Watanabe, M.; Wiorkiewicz-Kuczera, J.; Yin, D.; Karplus, M., *J. Phys. Chem. B* 1998, 102, 3586-3616.

32. Gaussian 03, Revision C.02, Frisch, M. J.; Trucks, G. W.; Schlegel, H. B.; Scuseria, G. E.; Robb, M. A.; Cheeseman, J. R.; Montgomery, Jr., J. A.; Vreven, T.; Kudin, K. N.; Burant, J. C.; Millam, J. M.; Iyengar, S. S.; Tomasi, J.; Barone, V.; Mennucci, B.; Cossi, M.; Scalmani, G.; Rega, N.; Petersson, G. A.; Nakatsuji, H.; Hada, M.; Ehara, M.; Toyota, K.; Fukuda, R.; Hasegawa, J.; Ishida, M.; Nakajima, T.; Honda, Y.; Kitao, O.; Nakai, H.; Klene, M.; Li, X.; Knox, J. E.; Hratchian, H. P.; Cross, J. B.; Bakken, V.; Adamo, C.; Jaramillo, J.; Gomperts, R.; Stratmann, R. E.; Yazyev, O.; Austin, A. J.; Cammi, R.; Pomelli, C.; Ochterski, J. W.; Ayala, P. Y.; Morokuma, K.; Voth, G. A.; Salvador, P.; Dannenberg, J. J.; Zakrzewski, V. G.; Dapprich, S.; Daniels, A. D.; Strain, M. C.; Farkas, O.; Malick, D. K.; Rabuck, A. D.; Raghavachari, K.; Foresman, J. B.; Ortiz, J. V.; Cui, Q.; Baboul, A. G.; Clifford, S.; Cioslowski, J.; Stefanov, B. B.; Liu, G.; Liashenko, A.; Piskorz, P.; Komaromi, I.; Martin, R. L.; Fox, D. J.; Keith, T.; Al-Laham, M. A.; Peng, C. Y.; Nanayakkara, A.; Challacombe, M.; Gill, P. M. W.; Johnson, B.; Chen, W.; Wong, M. W.; Gonzalez, C.; and Pople, J. A.; Gaussian, Inc., Wallingford CT, 2004.

33. Fender, B. J.; Short, K. W.; Hahn, D. K.; Callis, P. R., *Int. J. Quantum Chem.* 1999, 72, 347-356..

34. Short, K. W.; Callis, P. R., *J. Chem. Phys.* 2000, 113, 5235-5244.

35. Marcus, R. A., *J. Chem. Phys.* 1965, 43, 679-701.

36. Callis, P. R.; Vivian, J. T.; Slater, L. S., *Chem. Phys. Lett.* 1995, 244, 53-58.

37. Callis, P. R.; Petrenko, A.; Muino, P.; Tusell, JR, *J. Phys. Chem. B* 2007, 111, 10335-10339.

38. Bixon, M.; Jortner, J., *Adv. Chem. Phys* 1999, 106, 35-202.

39. Levich, V. G.; Dogonadze, R. R., *Dokl. Akad. Nauk USSR* 1959, 124, 123-126.

40. Kestner, N. R.; Logan, J.; Jortner, J., *J. Phys. Chem.* 1974, 78, 2148-2166.

# APPENDICES

# APPENDIX A

## DENSITY OF STATES FOR FLAVIN – TYROSINE

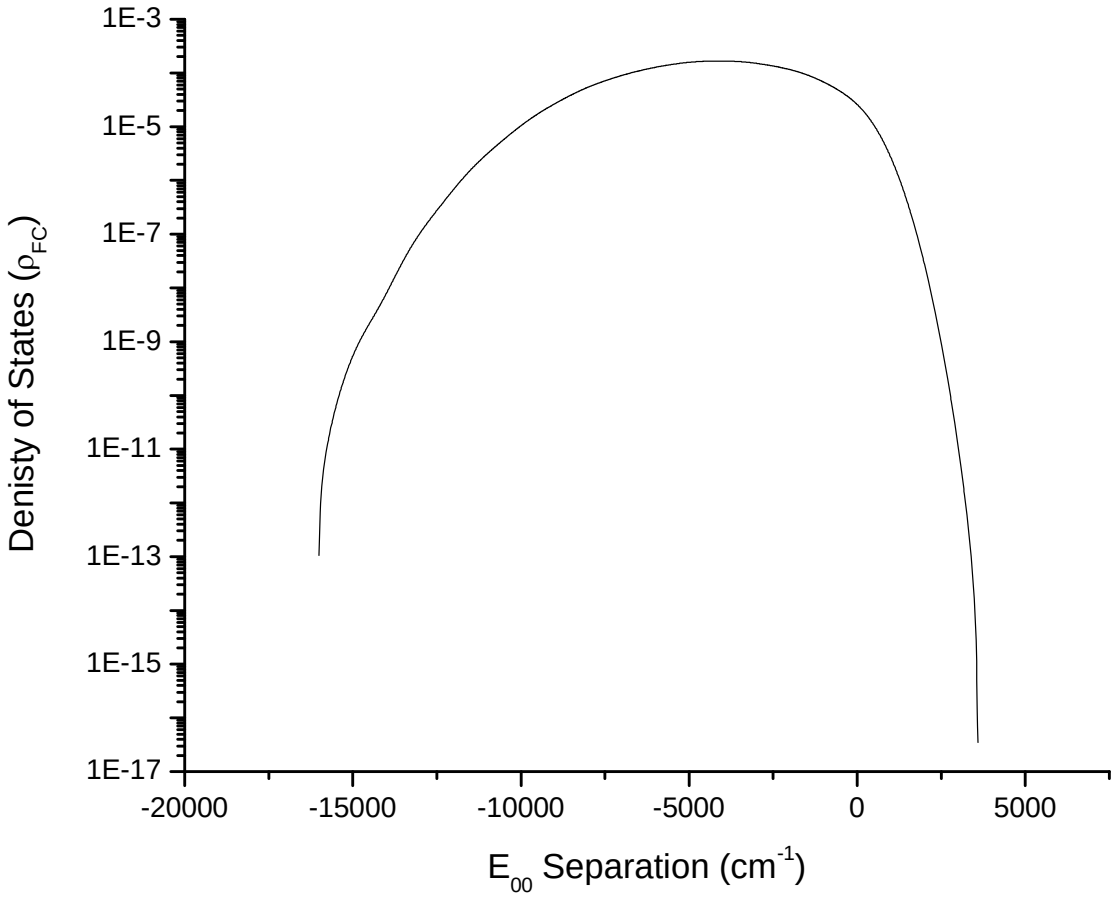
1E-3
1E-5
1E-7
1E-9
1E-11
1E-13
1E-15
1E-17
Denisty of States ($\rho_{FC}$)
-20000
-15000
-10000
-5000
0
5000
$E_{00}$ Separation ($cm^{-1}$)

# APPENDIX B

## DENSITY OF STATES FOR FLUORESCEIN – TYROSINE

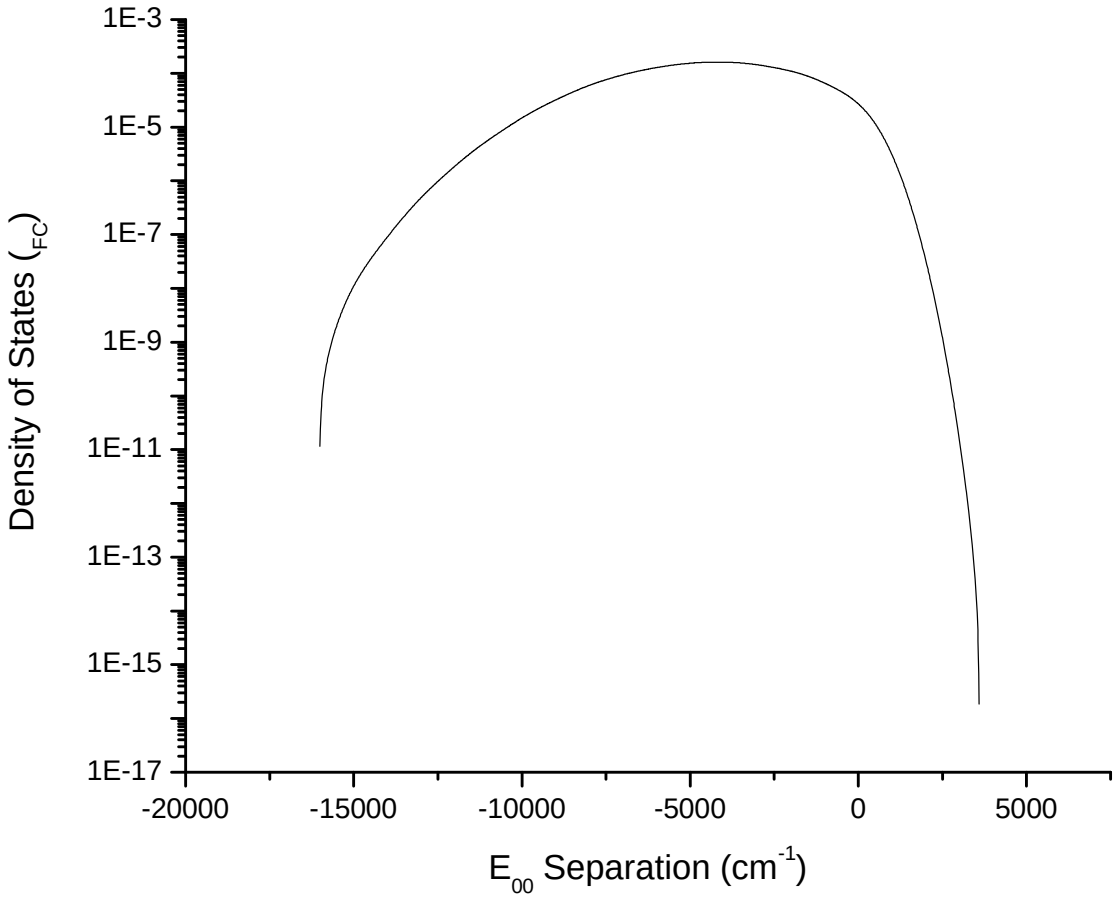
1E-3
1E-5
1E-7
1E-9
1E-11
1E-13
1E-15
1E-17
Density of States ($_{FC}$)
-20000
-15000
-10000
-5000
0
5000
$E_{00}$ Separation ($cm^{-1}$)

# APPENDIX C

## DENSITY OF STATES FOR FLUORESCEIN – TYROSINE

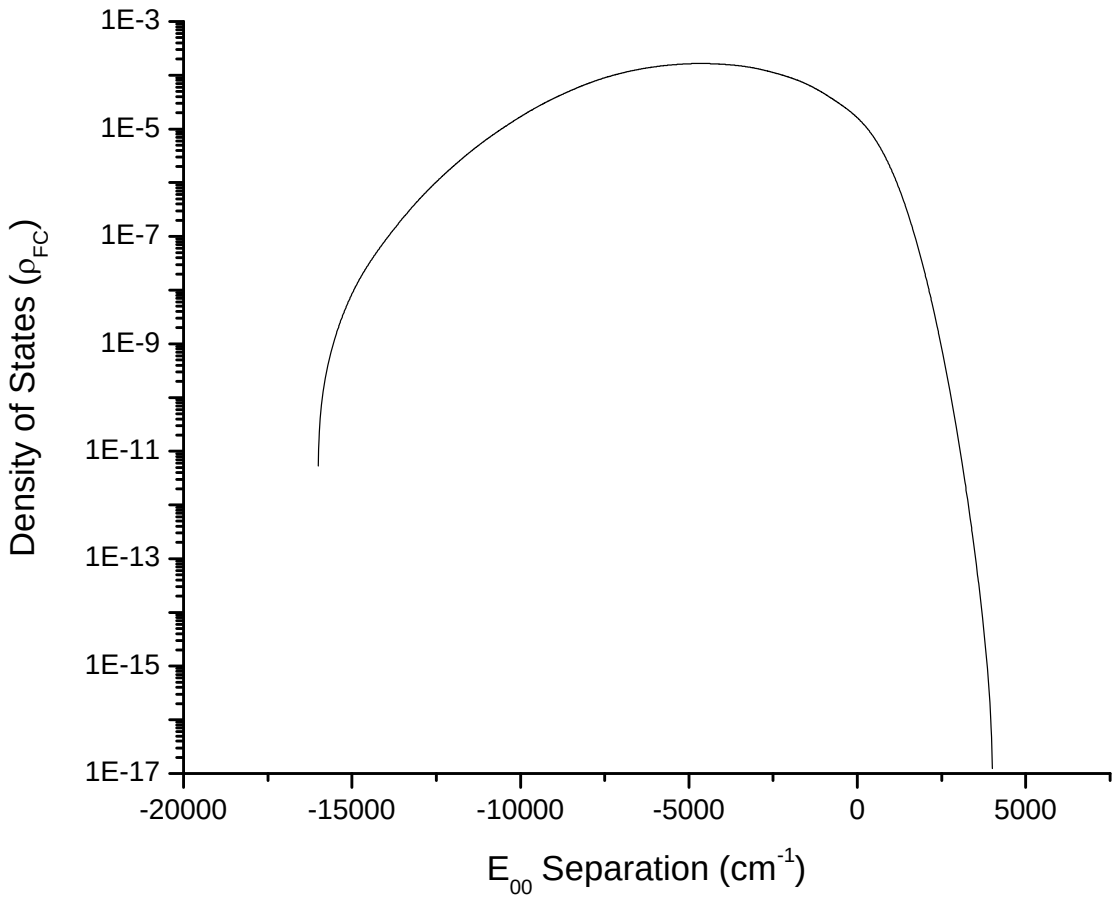
1E-3
1E-5
1E-7
1E-9
1E-11
1E-13
1E-15
1E-17
Density of States ($\rho_{FC}$)
-20000
-15000
-10000
-5000
0
5000
$E_{00}$ Separation ($cm^{-1}$)